Renewable Energy 109 (2017) 576–585

Contents lists available at ScienceDirect

Renewable Energy

journal homepage: www.elsevier.com/locate/renene

Performance evaluation of building integrated solar thermal shading system: Active solar energy usage

Li Li [a], Ming Qu [a, *], Steve Peng [a, b]

[a] School of Civil Engineering, Purdue University, 550 Stadium Mall Dr. CIVL G243, West Lafayette, IN, United States
[b] California State University, East Bay, United States

ARTICLE INFO

Article history:
Received 21 September 2016
Received in revised form
21 February 2017
Accepted 19 March 2017
Available online 27 March 2017

Keywords:
BISTS
Solar fraction
Solar useful efficiency
DHW
Space heating
Space cooling

ABSTRACT

This paper presents an evaluation of the building integrated solar thermal shading (BISTS) system on solar energy usage. A medium office building in Los Angeles defined by the U.S. Department of Energy (DOE) was used in the case study. The BISTS louvers mounted on the south, east, and west façades of the building were used to harvest solar energy to supply domestic hot water (DHW), space heating and/or cooling. The solar thermal system was modeled and simulated in TRNSYS. Solar fraction and solar useful efficiency were calculated, and a recommended operation strategy was proposed. The results indicated that: 1) potentially, the annual domestic hot water load can be fully supplied by the BISTS system. To achieve a recommended solar fraction 75%, either 10 m^2 collector on the south façade or 33 m^2 collector on the east and west façades are required; 2) 20.2% of cooling load or 64.6% of heating load can be met by the remaining collectors. The BISTS on the south façade is primarily recommended to provide space heating and/or cooling; 3) combined heating and cooling enables the system to take more advantage of solar energy for energy savings from auxiliary heating.

1. Introduction

Currently, solar technology has been used in a variety of applications, such as solar water heating, solar space heating and cooling, solar refrigeration, solar desalination, solar thermal power, and solar furnaces [1]. The integration of solar systems to the building envelope has attracted increasing attentions as it provides a new solution to reduce fossil fuel consumption and greenhouse gas emissions by taking advantage of renewable energy [2]. There are several ways to implement a solar system to a building. Some solar systems are separated elements that are added to the building after construction, some solar systems replace the building elements thereby serving multiple functions. The integrated solar thermal collectors are commonly located on roofs [3,4], façades [5,6], gutters [7–9], and shadings [10]. Building integrated solar thermal shading (BISTS) system is a new type of solar thermal application that potentially replaces traditional building exterior shading devices with small-sized solar thermal collectors for thermal heat generation, solar heat gain reduction, and glare control.

Buildings are responsible for 41% of the country's primary energy use in the United States. Of all the energy consumed by buildings, space heating, space cooling, water heating, and lighting account for over 60% [11]. The BISTS system can not only absorb solar energy for space heating, space cooling, and water heating, but also influence the interior daylight condition and visual comfort. However, the studies about the BISTS systems have not been widely reported [12]. Palmero-Marrero et al. [10] evaluated the potential of an integrated solar louver collector system for water heating in EES, which is a general equation-solving program that can numerically solve thousands of coupled non-linear algebraic and differential equations [13]. Different collector configurations were analyzed. Up to 83% of annual solar fraction was obtained for Lisbon and 95% for Tenerife. The building energy requirements and temperature behaviors were also calculated [14]. However, this analysis considered only the south-oriented horizontal louvers and it was based on a single-zone building.

Although the study about the BISTS system is limited, many other building solar systems have been evaluated. Some research focused on the life cycle analysis [7,8], and some other investigated the thermal and/or energetic behavior of the solar systems. Both experimental and modeling methods have been used in previous studies. For a yearly performance prediction, practical test is time

* Corresponding author.
E-mail address: mqu@purdue.edu (M. Qu).

http://dx.doi.org/10.1016/j.renene.2017.03.069
0960-1481/

consuming, expensive and difficult to be adopted because it may take long periods of time to obtain test results [15]. Many modeling programs, such as TRNSYS, WATSUN, Polysun, and F-Chart are used for the performance prediction of solar energy systems with their acceptable accuracy [16]. Oishi et al. [15] used TRNSYS to model and evaluate the performance of three types of representative solar DHW systems in Japan. Simulation results of water temperature behavior were compared with the practical indoor/outdoor testing data and revealed that the errors were less than 6%. Matuska et al. [6] compared the thermal behavior of façade-integrated collectors with standard roof-located collectors for water heating in a block of flats with TRNSYS simulation. The study reported that façade solar collectors should have an area increased by approximately 30% to achieve the usual 60% solar fraction, which is defined as the percentage of heat load that is met by solar energy [10], compared with conventional roof solar collectors with a 45° slope. This is because façade-integrated solar system has limitation to adjust the slope angle, resulting in reduction in irradiation reception.

Most building solar systems were employed for domestic hot water usage. Compared to space heating and cooling, DHW load is small and constant all year round and the system is not very complex to integrate. Kalogirou [17] conducted a feasibility study for the use of solar parabolic trough collectors for hot water production in Cyprus for both domestic and hotel applications. The systems were optimized using the F-Chart program and compared to similar systems using flat plate collectors. Monthly and annual solar fractions were computed and the results showed that for large scale water production, the parabolic trough collectors were more efficient than the flat plate ones. Some solar systems supply both DHW and space heating. Hassan et al. [4] studied a roof-integrated solar collector on a typical two or three story building in Blacksburg. 3D finite element models were developed in ABAQUS software to evaluate the thermal performance. The results concluded that the energy collected is sufficient to satisfy about 85% of the building space heating and hot water requirements. Recently, the application of solar absorption chiller or solar adsorption chiller makes it possible to use solar energy to provide space cooling. And the solar cooling systems have been applied to different building types, including offices, schools, hospitals, and hotels [18]. Florides et al. [19] modeled a lithium bromide – water absorption solar cooling system in TRNSYS for a typical house in Cyprus. A system optimization in terms of energy gain and life cycle savings was carried out to select the optimum tank size, collector type, collector slope and area, thermostat setting of the auxiliary boiler. Hang et al. [20] presented an optimization of solar cooling system considering the solar fraction and budgets limits. The central composite design approach was used to reduce the number of experimental trials and the simulations were carried out in TRNSYS. A case study based on a small-sized office building in West Lafayette was conducted to verify the simulation results.

Although solar thermal systems have potential to provide free energy for DHW, space heating, and space cooling, few research combined these three applications in one study to evaluate. In addition, since it is not easy to integrate solar collectors as shading devices in terms of esthetic and structural consideration, limited scientific results are available for helping decision making of BISTS design and operation. Motivated by the above reasons, this paper presents a case study to predict the performance of the BISTS system on solar energy usage, as the second paper of BISTS system evaluation.

2. Research approach and evaluation indicators

A case study was carried out to evaluate the solar energy usage of the BISTS system based on an application to a medium office reference building from the U.S. Department of Energy (DOE) located in Los Angeles, CA [27]. The BISTS were placed on the south, east, and west windows to provide DHW, space heating and/or cooling of the building in the study. As the DHW load is relatively constant, the BISTS system is primarily employed to provide domestic hot water. The rest BISTS collectors are either used for space heating, cooling, or both. Various system configurations and different operation strategies were investigated and analyzed by using building and energy system simulation in TRNSYS, which is a transient systems simulation program with a modular structure developed at the University of Wisconsin by the solar energy laboratory [34]. TRNSYS platform has been validated by many studies to provide accurate results with less than 10% error between the simulation results and the measured data [21].

The east BISTS are considered to work in the morning before 12 p.m. of solar time and the west BISTS are considered to work from 12 p.m. of solar time to the end of the afternoon since the west-facing collectors are blocked by the building itself from receiving solar radiation in the morning and likewise for the east-facing collectors in the afternoon. The BISTS were installed symmetrically on the east and west façades, therefore this study assumes that either the eastern or western BISTS operates during a day. In this way, we do not need to consider the variation of solar heat flux from the morning to the afternoon. For the south collectors, they have solar accessibility during daytime.

Solar Fraction and Solar Useful Efficiency were used as the indicators of system performance. Solar Fraction (F_{solar}) is the ratio of the energy contributed by solar source to the total load requirement. It can be calculated as equation (1).

$$F_{solar} = \frac{Q_{useful}}{Q_{load}} = 1 - \frac{Q_{aux}}{Q_{load}} \tag{1}$$

where,

Q_{load}: total thermal load [kJ];
Q_{useful}: thermal energy from the solar source [kJ];
Q_{aux}: thermal energy from the auxiliary heater [kJ].

Solar energy gained from the collectors sometimes cannot be fully used due to heat loss and mismatch with load demands. Solar Useful Efficiency (η_{solar}) is hence employed to determine the percentage of the collected solar energy that has been effectively used. It is calculated as the ratio of the useful solar energy and the total solar energy gain from the collectors, as shown in equation (2).

$$\eta_{solar} = \frac{Q_{useful}}{Q_{gain}} \tag{2}$$

where,

Q_{useful}: thermal energy from the solar source [kJ];
Q_{gain}: total solar energy gain from solar panels [kJ].

3. Collector information

The prototype panel of the studied BISTS collector is 210 mm wide and 51.5 mm thick, and the length can be customized. The main housing is made of 2 mm polycarbonate. And the top and bottom surfaces are oval curved. The panel core is 10 mm thick for fluid flow through. The lower portion has 25 mm polyurethane foam insulation, with heat conductivity of 0.03 W/(m × K). The upper portion has 10 mm air layer. The cross section of a BISTS prototype and the installation layouts are schematically shown in

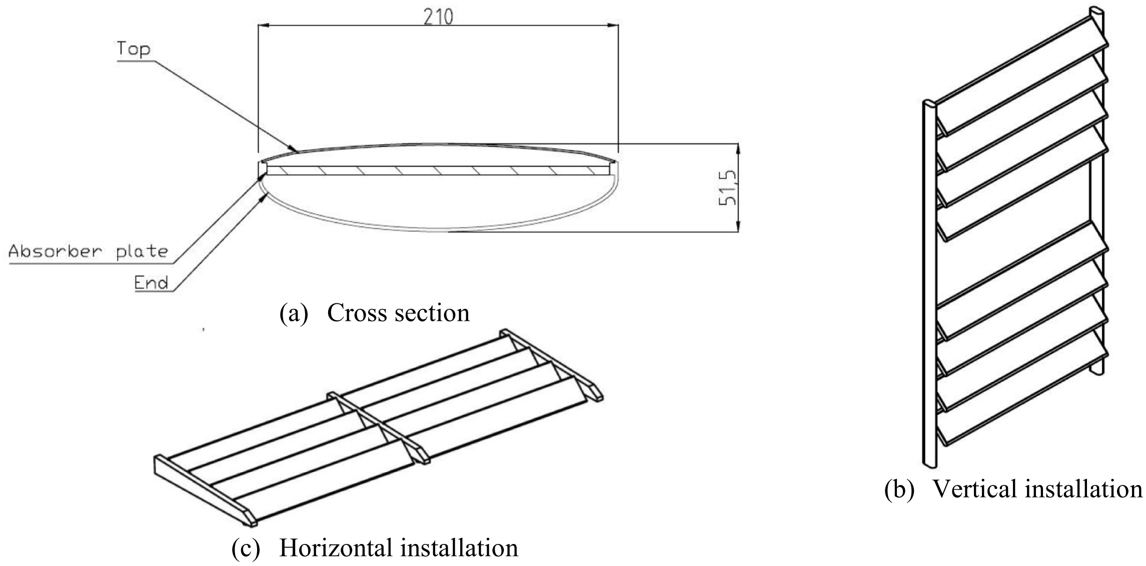

Fig. 1. BISTS cross section and installation layouts.

Fig. 1.

According to the manufacturer, the thermal performance of the studied BISTS prototype is similar with a certified flat plate solar collector model EC-40-1.5 [22]. This model has been tested according to the Solar Rating & Certification Corporation (SRCC) Standard 100-2005-09. SRCC is an independent third-party certification organization that administers national certification and rating programs for solar energy equipment. It provides rating information to help compare the efficiency of various solar collectors on the market [23]. Therefore, the SRCC test data for the model EC-40-1.5 has been adopted in this study for BISTS evaluation. The collector efficiency depends on the solar intensity and the fluid temperature. A general way to calculate the collector efficiency is to use the Hottel-Whillier equation (3) [24]. The efficiency vs. ΔT curve (Fig. 2) can be modeled as a quadratic correlation, where ΔT is the difference between the collector inlet fluid temperature and the ambient air temperature; I_g is the global solar incidence (Fig. 3). The maximum optical efficiency of the studied collector is 75%, which is reasonable for a typical glazed flat-plate collector [25].

$$\eta = \frac{Q_u}{A_c I_g} = F_R(\tau\alpha)_n - F_R U_L \frac{(T_i - T_a)}{I_g} - F_R U_{L/T} \frac{(T_i - T_a)^2}{I_g} \tag{3}$$

where,

Q_u: solar energy gain [kJ];
A_c: total collector array aperture or gross area [m^2];
I_g: global solar radiation incident on the solar collector [kJ/h × m^2];
T_i: inlet fluid temperature [°C];
T_a: ambient temperature [°C];
F_R: overall collector heat removal factor. F_R is the ratio of the actual useful energy gain to the energy gain calculated assuming that the collector plate temperature is always equal to T_i;
U_L: overall thermal loss coefficient of the collector per unit area [kJ/h × m^2 × K];
$U_{L/T}$: thermal loss coefficient dependency on T [kJ/h × m^2 × K^2];
τ: short-wave transmittance of the collector covers;

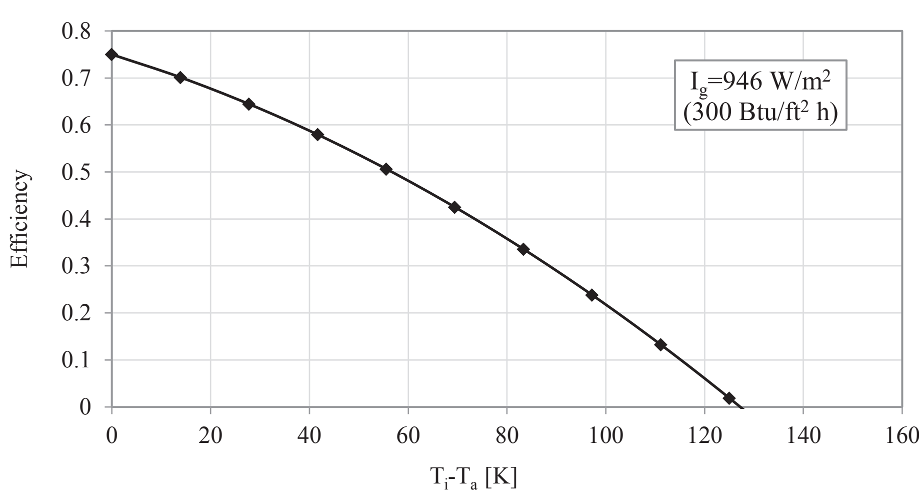

Fig. 2. Collector efficiency performance.

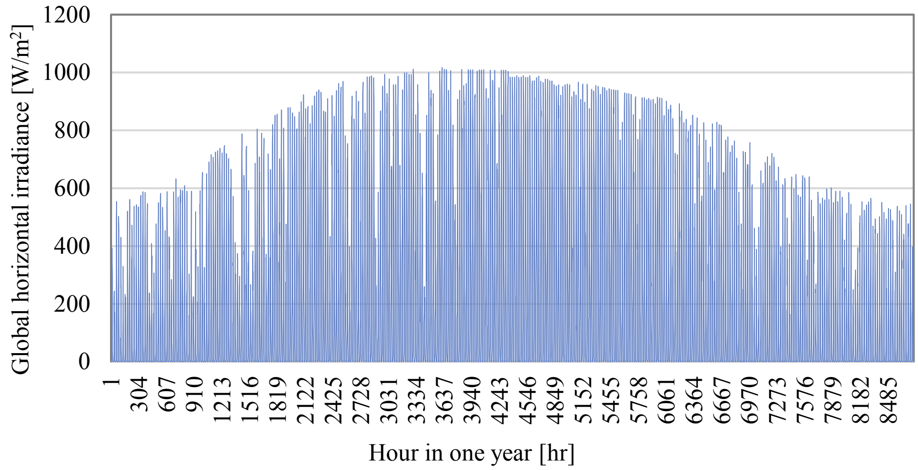

Fig. 3. Global horizontal irradiance (total amount of direct and diffuse solar radiation received on a horizontal surface) in Los Angeles.

α: short-wave absorptance of the absorber plate;
$(\tau\alpha)_n$: product of the cover transmittance and the absorber absorptance at normal incidence;

The performance of a collector was tested on clear days at normal incidence. In reality, solar radiations do not always incident at a normal direction, but at an incident angle. Therefore, the collector efficiency has to be corrected for non-normal solar incidence by the incident angle modifier (IAM) K_θ (Fig. 4) [22]. The IAM is defined as the efficiency at a given incident angle divided by the efficiency at normal incidence [26].

The collector performance may also vary with the changes in flow rate. Many recommendations exist with respect to the flow rate through solar collectors. For glazed flat-plate liquid-type solar collectors, the flow rate per unit area recommended by ASHRAE standard is 0.02 kg/(s $\times$ m^2) [23], and is at a range of 0.025 gpm/sf to 0.075 gpm/sf [27], which is 0.017 kg/(s $\times$ m^2) to 0.051 kg/(s $\times$ m^2), recommended by collector manufacturers. In this study, the test mass flow rate is 0.0201 kg/(s $\times$ m^2) according to the SRCC test report [22].

4. Building model and BISTS configuration

A medium office reference building from the DOE [28] was used as our study case. DOE has developed and maintained a suite of 16 prototype building models that represent approximately 70% of the commercial buildings across 16 locations, which represent all U.S. climate zones. The studied building is a three-story office located in Los Angeles with a total floor area of 4983 m^2 and a window fraction of 0.33. The dimension of the building is 49.91 m (length) $\times$ 33.27 m (width) $\times$ 11.89 m (height). The reference building complies with the minimum requirements of ANSI/ASHRAE/IES Standard 90.1–2010, including the envelope, lighting, heating, ventilation and air conditioning systems [29], which provides a consistent baseline for BISTS application and comparison.

The BISTS system was implemented on the south, east, and west façades of the building, as shown in Fig. 5a. Considering the shading effects, horizontal layout was determined to be installed to the south façade, and vertical louvers were integrated to the east and west façades [14,30]. For simplification, the panel surfaces were considered as flat and the length of panel was equal to the width of window during the modeling process.

The space between two adjacent panels was designed to be 0.21 m so that the louvers can be completely closed at certain slat angles, as shown in Fig. 5 (b) and (c). Parametric study has been conducted in previous research to determine a final BISTS design [30], in which the total depth d, the height above the window h, the shading-to-window ratio r, and the slat angle θ were discussed and

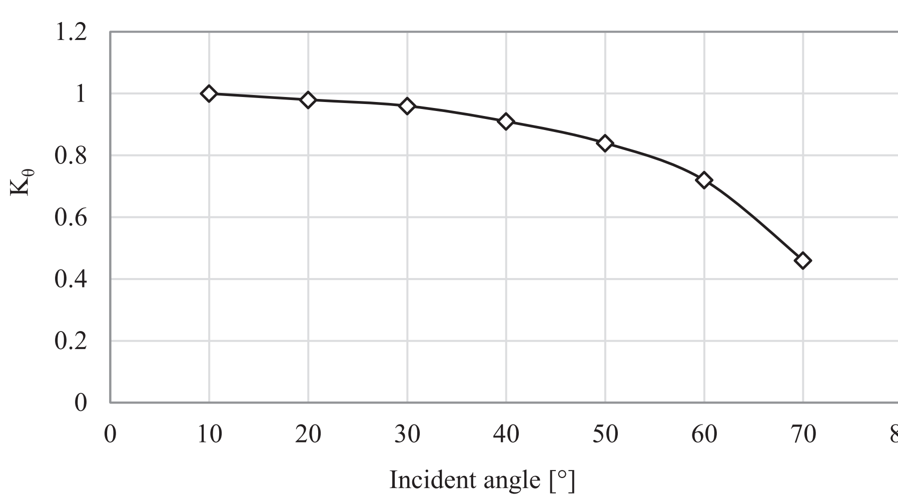

Fig. 4. Incident angle modifier.

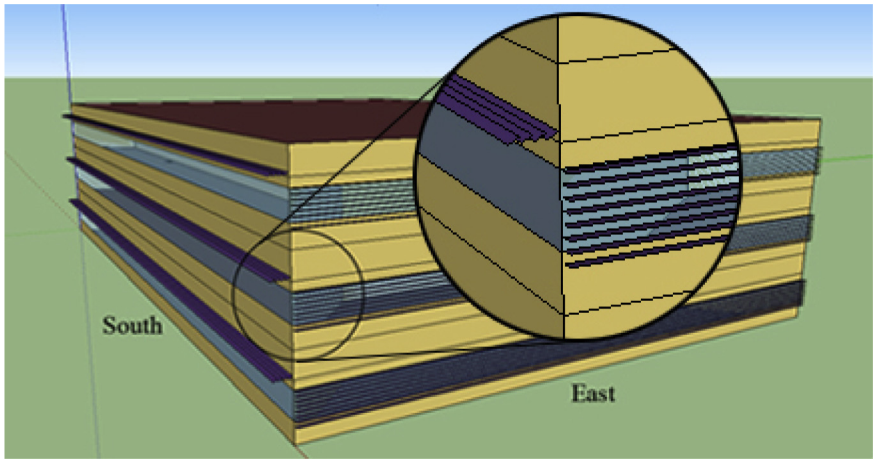

(a) Overview

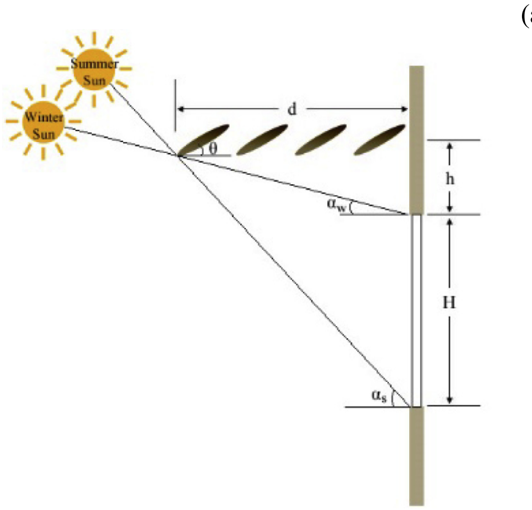

(b) Configuration detail: horizontal (south façade)

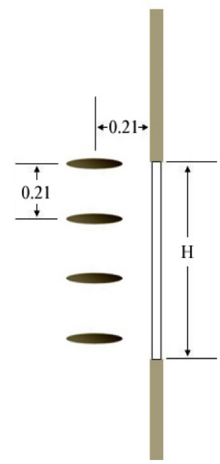

(c) Configuration detail: vertical (east and west facades)

Fig. 5. BISTS configuration.

determined by considering the building energy consumption and daylight provision. Various *d*-*h*-*θ* and *r*-*θ* combinations were simulated. Accordingly [30], for the horizontal BISTS, case "d0.84_h0.66_30°" was selected because it shows outstanding performance on primary energy saving and daylight condition improvement. Therefore, 4 panels were placed on each strip window horizontally with 30° surface slope on the south façade and the total collector area on the south façade was about 125 m^2. The depth of the BISTS was 0.84 m and it was located 0.66 m above the window. For the vertical BISTS, it was recommended to fully cover the window, and 0° slat angle helps to redirect the sunlight into the deeper space of the room [30]. Thus, case "r1.28_0°" was used on both east and west façades. 48 panels were symmetrically mounted vertically with 0° slat angle (8 panels on each strip window) and the shading-to-window ratio was 1.28. The collector area was about 167.5 m^2 on each side. In summary, the total collector area installed on the building was 460 m^2, as detailed in Table 1.

Table 1
BISTS configuration.

Orientation	Configuration	# of panel	Slat angle	Collector area [m^2]
South	d0.84_h0.66_30°	12	30°	125
East	r1.28_0°	24	0°	167.5
West	r1.28_0°	24	0°	167.5
Total		60		460

Note: In the names of configuration, *d* is the horizontal depth of the overhang; *h* represents the vertical height of the overhang above the window; *r* is the shading-to-window ratio. For the surface slope of the solar panel, 0° is horizontal and 90° is vertical.

5. Energy supply systems

5.1. DHW heating system

The hot water system employs the BISTS system to absorb solar energy and to convert it to thermal energy in water. The DHW system for the case study consists of a tank, solar collectors, and an auxiliary heater, as shown in Fig. 6. The circulating water from the bottom of the storage tank is pumped to the solar collectors. The pump sets the flow rate for the rest of the components in the flow loop. An on/off controller turns the pump on when the collector outlet temperature is higher than the inlet temperature, and turns the pump off once the collector outlet temperature drops below the inlet temperature. The solar energy collected by the collectors is then carried by the circulating water and stored in the storage tank. The stratified tank with various inlets has five fully-mixed layers with initial temperature of 60 °C, 50 °C, 40 °C, 30 °C, and 20 °C, from top to bottom. The city water at temperature around 20 °C, as make-up water, enters the tank from the bottom. Two auxiliary heaters are located at the topmost layer in the tank, which will be

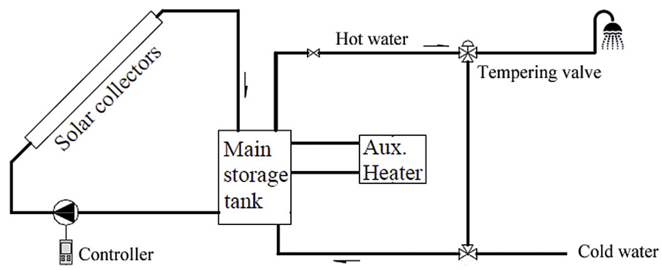

Fig. 6. Schematic diagram of the solar DHW system.

energized when the node temperature falls below the set-point. If the tank temperature reaches the boiling temperature at 100 °C, steam is assumed to be vented to keep the fluid at the boiling temperature. A tempering valve controls the flow rate of the main stream and the bypass stream so that the mixed fluid temperature will not exceed the set-point of the supply temperature 45 °C. Table 2 lists the parameter settings for the simulation of the solar DHW system.

Fig. 7 is the weekly DHW profile of the medium office reference building, predicted by the DOE through the system simulations conducted in EnergyPlus [27]. The maximum flow rate is 128 kg/hr and the minimum load is 9 kg/hr.

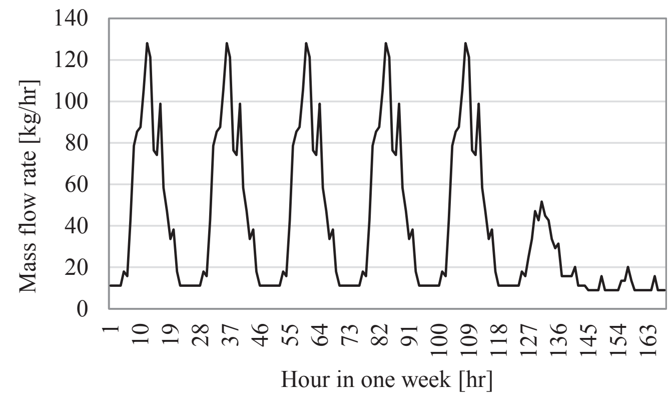

Fig. 7. Domestic hot water load in one week.

5.2. Solar cooling and heating system

A solar absorption cooling and heating (SACH) system was implemented by using the BISTS system to supply space heating and/or cooling. The SACH system, as shown in Fig. 8, is composed of solar collectors, a storage tank, an auxiliary heater and an absorption chiller. The solar field collects solar energy, which is then converted into thermal energy and stored in the main tank. The controller turns the pump on or off according to the temperature difference between collector inlet and outlet. A storage tank is equipped to stabilize the operation of the system since the solar energy is not always available or in phase with the heating or cooling load [31]. The tank size is 17.5 m^3 and the initial temperatures of water at different heights of the stratified tank are assumed to be 90 °C, 85 °C, 80 °C, 75 °C, and 70 °C, from top to bottom. The supply temperature set point is 90 °C. An auxiliary heater is installed to maintain the set point temperature and provide the compensation if the solar energy is not adequate, thus the absorption chiller can always cover the required heating or cooling load without equipping an additional electricity-driven chiller. The dead band is 5 °C to initiate the auxiliary heater.

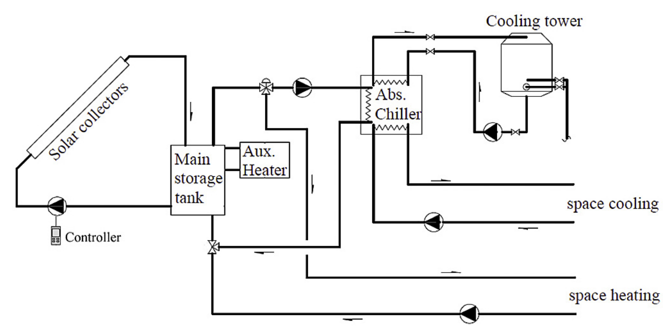

Fig. 8. Schematic diagram of the solar absorption cooling and heating system.

The heating and cooling loads of the medium office building with the BISTS application were predicted by EnergyPlus simulation from previous study [30]. Accordingly, the total heating energy is 3.94 × 10^7 kJ with a peak load of 368,361 kJ/h and the total cooling energy is 9.40 × 10^8 kJ with a peak load of 933,283 kJ/h. The building in Los Angeles, as noticed, is cooling dominated and has cooling loads all year around (Fig. 9).

According to the building load demands, the collected solar energy can be directly used for space heating, or used by a single-effect H_2O/LiBr absorption chiller for space cooling. The heating and cooling modes are controlled by a diverter, which splits one fluid stream from tank outlet into two possible streams according to the control signal. For heating mode, the fluid runs only in the heating loop. And for cooling mode, the fluid all goes to the cooling loop. When it has both heating and cooling loads, the mass flow rate of each fluid stream is determined depending on dynamic heating and cooling demand ratios. Parameter settings for the SACH system simulation are listed in Table 3.

Table 2
Parameter settings for solar DHW system.

Component	Parameter	Value
Fluid properties	Fluid specific heat [kJ/kg × K]	4.19
	Tested flow rate [kg/hr × m^2]	72.36
Flat-plate collector	Intercept efficiency	0.75
	Efficiency slope [kJ/hr × m^2 × K]	10.955
	Efficiency curvature [kJ/hr × m^2 × K^2]	0.07176
	1st order IAM	0.28
	2nd order IAM	0
Stratified storage tank	Tank loss coefficient [kJ/hr × m^2 × K]	2.5
	Set point temperature [°C]	60
	Dead band for set point [Δ°C]	10
	Maximum heating rate [kJ/hr]	9000
	Boiling point [°C]	100
Pump and controller	Maximum power [kJ/hr]	60
	Conversion coefficient	0.05
	Power coefficient	0.5
	Upper dead band ΔT_H	5
	Lower dead band ΔT_L	2

6. Results and discussion

6.1. DHW heating

The BISTS system is primarily employed for the DHW heating because the load is small and constant. The results of solar fraction and solar useful efficiency are plotted as a function of collector area as displayed in Fig. 10. The solar fraction increases along with the collector area while the solar useful efficiency decreases. For the BISTS on the south façade, 40 m^2 area is enough to satisfy over 99% of domestic hot water demand. Continuing to increase the collector

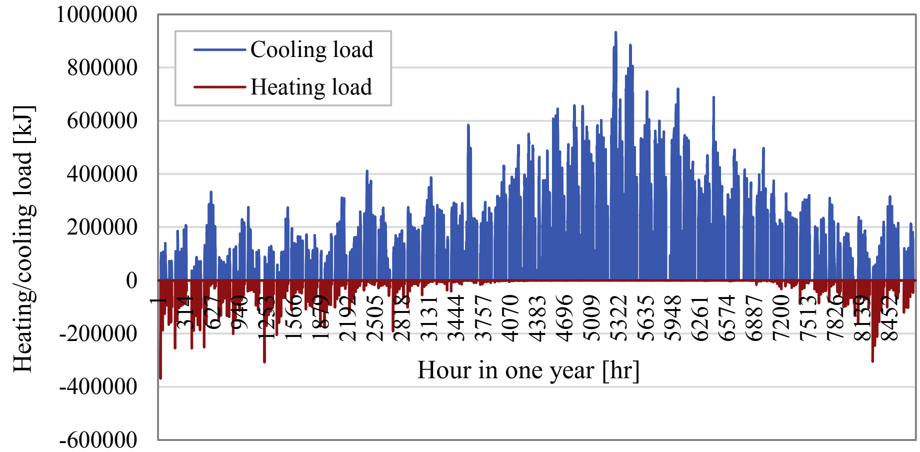

Fig. 9. Annual hourly space heating and cooling loads.

Table 3
Parameter settings for solar heating and cooling system.

Component	Parameter	Value
Absorption chiller	Chilled water set point [°C]	6.7
	Chilled water flow rate [kg/hr]	40,000
	Cooling water inlet temperature [°C]	22
	Cooling water flow rate [kg/hr]	30,000
	Hot water inlet temperature [°C]	90
	Hot water flow rate [kg/hr]	8000
	Rated COP	0.53
Stratified storage tank	Set point temperature [°C]	90
	Dead band for set point [Δ°C]	5
	Maximum heating rate [kJ/hr]	2,000,000
	Boiling point [°C]	100

area on top of that does not significantly help to improve the solar fraction but would keep reducing the solar useful efficiency. Although 100 m^2 of BISTS collectors on the south façade can potentially provide 100% of solar energy for domestic hot water heating, the solar useful efficiency is only 45% under this circumstance, in which more than half of collected solar energy has not been used. For the BISTS on the east and west façades, 100 m^2 collectors on the east and west façades in total can provide 99% of free solar heating energy but only 60% available solar energy is used.

According to the U.S. DOE, typical solar fractions for domestic hot water heating are 0.5–0.75 [32]. Walker [33] reported that the economic optimum is approximately 0.75. To achieve the optimal solar fraction, it is concluded that either 10 m^2 of south collectors or 33 m^2 of east and west collectors will be the economic optimal size. Thus, the available area of BISTS will be more than the needs from DHW. In order to avoid wasting the available BISTS, it is necessary to explore more usages for the remaining collectors. Space heating and cooling would be two potential possibilities.

6.2. *Space heating and/or cooling*

As concluded aforementioned, either 10 m^2 of south collectors or 33 m^2 of east and west collectors as one of two scenarios can be used to satisfy the desired DHW demands in the study of space heating and/or cooling as shown in Table 4. In the first scenario, 10 m^2 of south collectors is able to provide 74.4% of DHW by using solar energy and the remaining collectors of 115 m^2 on the south plus 335 m^2 on the east and west are used for space heating and/or cooling. On the other hand, for the second scenario, 33 m^2 of east and west collectors (16.5 m^2 on each side) provides 75.5% of DHW load, and 125 m^2 of south collectors plus 302 m^2 of collectors on the

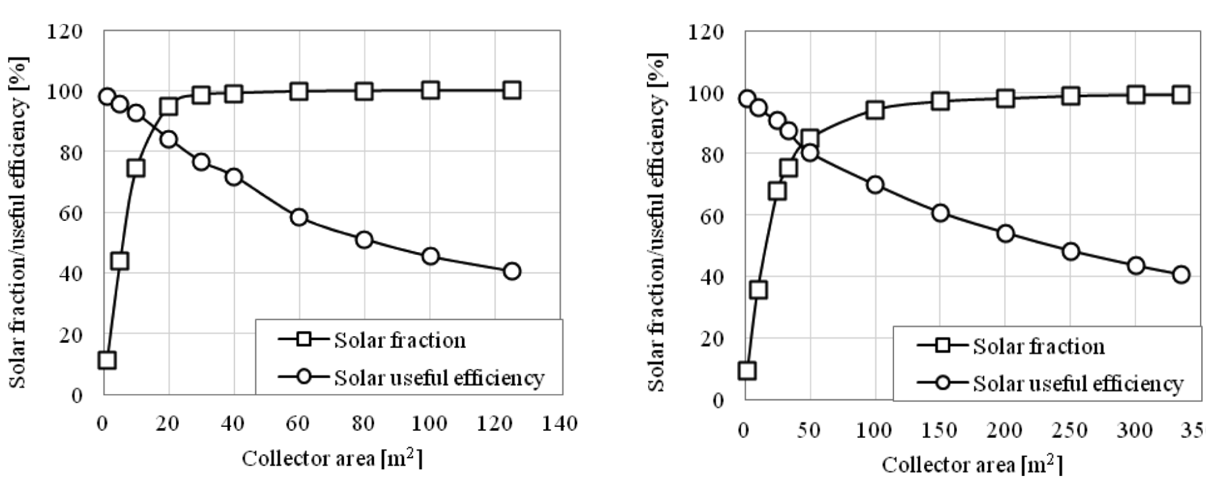

(a) South façade BISTS only

(b) East and west façades BISTS only

Fig. 10. Annual solar fraction and solar useful efficiency as a function of BISTS collector area for domestic hot water heating.

Table 4
Two study scenarios.

Scenario	Usage	Collector area [m^2]			
		South	East	West	Total
Scenario 1	Domestic hot water	10	0	0	10
	Space heating/cooling	115	167.5	167.5	450
Scenario 2	Domestic hot water	0	16.5	16.5	33
	Space heating/cooling	125	151	151	427

east and west supply space heating and/or cooling. Both scenarios have over 87% of solar useful efficiency for domestic hot water heating (Fig. 10).

The annual performance of the SACH system predicted by simulation model is shown in Table 5. Two scenarios are compared under three different modes: heating only, cooling only, and combined heating and cooling. For each mode, Scenario 1 achieves higher solar energy gain than Scenario 2 because it employs more collector area, especially on the east and west façades, for space heating and/or cooling. The energy gain is also influenced by the load demand, as noticed in the table. The higher the load demand is, the more solar energy is harvested from the collectors. This is because solar gain is proportional to the flowrate of the fluid in the solar collection loop. High load demand increases the flow rate of the fluid through the collector, resulting in more solar energy gain.

The solar energy collected from different oriented collectors has different effects on the load provision. East and west collectors harvest more energy in summer but less in winter, as shown in Fig. 11b. It is not helpful to improve the solar fraction for space heating because it is off phase with the heating load. On the other hand, solar energy collected by the south-facing collectors is relatively constant throughout a year (Fig. 11a), so that it is easier to supply both heating and cooling loads. Therefore, south-facing collectors are more favorable theoretically. This conclusion makes a good agreement with the data in Table 5. As shown, Scenario 2 is better than Scenario 1, considering both solar fraction and solar useful efficiency since Scenario 1 equipped more collector areas on the east and west façades and Scenario 2 has more collectors facing south. Therefore, Scenario 2 would be recommended as the final operation strategy.

For heating only mode, solar availability and heating load are not in phase. In summer, solar resource is abundant but there is no heating requirement, so that solar fraction can reach 100% from June to October but solar useful efficiency is almost zero (Fig. 12a). On the other hand, in winter, collected solar energy is not enough for heating, resulting only 40% of solar fraction in December and January.

In cooling only mode, solar energy is not enough to satisfy the large amount of cooling demand. The highest solar fraction is only around 35% in April and the lowest one is near 10% in December (Fig. 12b). The difference between two scenarios is not significant, and both scenarios have very high solar useful efficiency thanks to the accordance between solar gain and cooling profile. In August, the solar useful efficiency is about 94%, and over 50% in January.

Generally, system performance in combined heating and cooling mode is better than in either heating only mode or cooling only mode. First, the higher the load demand is, the more solar energy is harvested from the collectors. Combined heating and cooling mode obtained 2.5×10^8 kJ more solar energy than heating only mode, and 1.7×10^6 kJ more than cooling only mode. Second, more solar energy can be useful in combined mode since the SACH system can be run more constantly all year round for heating load in winter and cooling load in summer without wasting solar energy obtained, which leads to a higher solar useful efficiency (Table 5). However, the solar fraction is still low because the cooling load is dominant in Los Angeles. The annual load coverage is about 20% and the highest month is 35% in April (Fig. 12c).

7. Conclusion

This study evaluated the solar fraction and the solar useful efficiency of the BISTS system applied to a medium office building in Los Angeles. The BISTS collectors on the south, east, and west façades of the building were used to collect solar energy to supply domestic hot water, space heating and/or cooling for the building. The building and energy supply systems were modeled in TRNSYS.

Table 5
Performance comparison of two scenarios under different modes.

Mode	Scenario	Q_{gain} [kJ]	Q_{load} [kJ]	Q_{useful} [kJ]	F_{solar} [%]	η_{solar} [%]
Heating only	1	1.619E+08	3.94E+07	2.49E+07	63.1	15.4
	2	1.612E+08	3.94E+07	2.55E+07	**64.6**	15.8
Cooling only	1	4.091E+08	1.74E+09	3.52E+08	20.2	85.9
	2	4.086E+08	1.74E+09	3.52E+08	20.2	**86.0**
Combined heating and cooling	1	4.103E+08	1.78E+09	3.55E+08	20.0	86.5
	2	4.102E+08	1.78E+09	3.56E+08	**20.1**	86.8

The signification of bold indicates that Scenario 2 has better performance than Scenario 1.

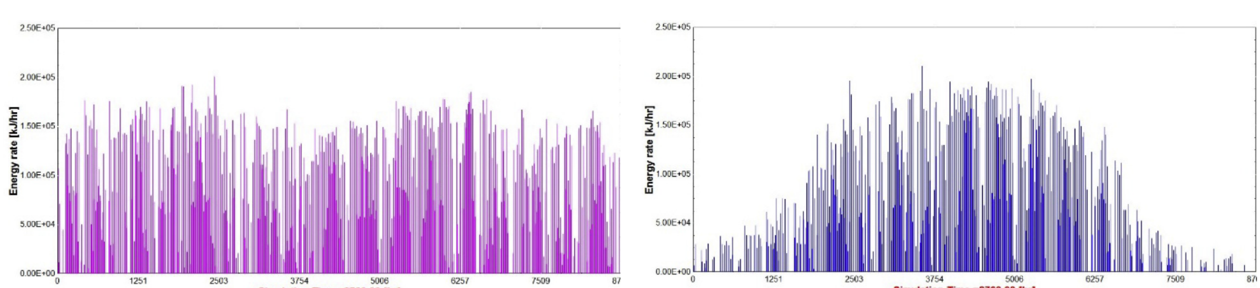

(a) South collectors (b) East and west collectors

Fig. 11. Energy gain profile from different oriented collectors.

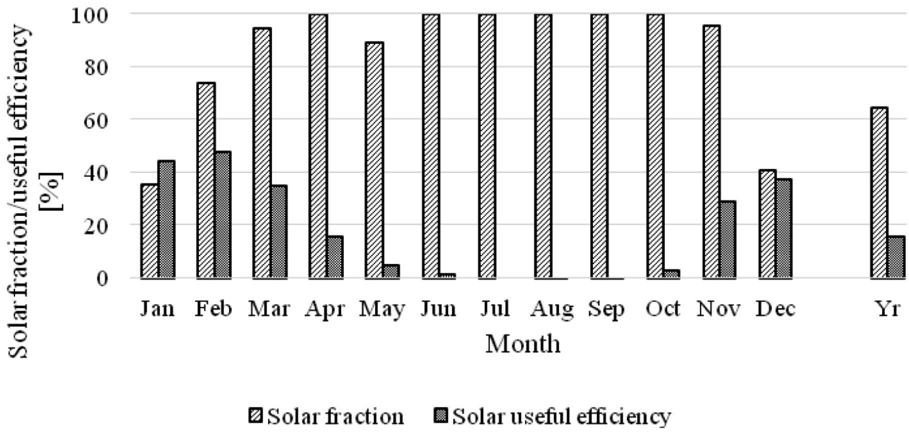

(a) Heating mode

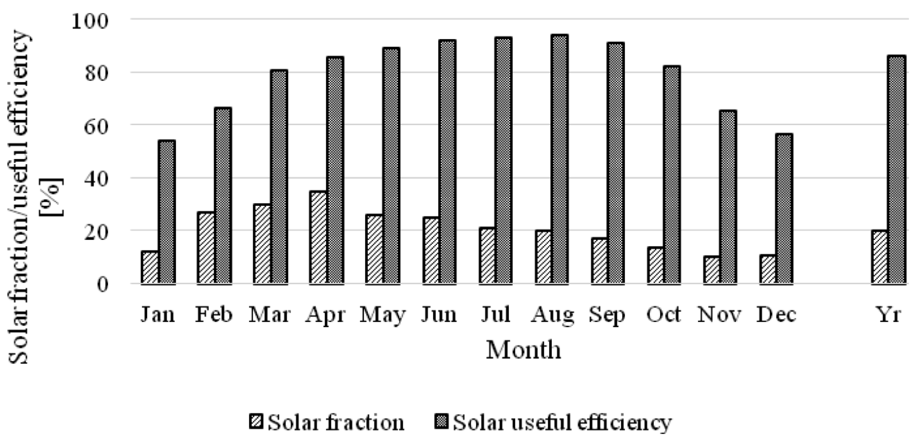

(b) Cooling mode

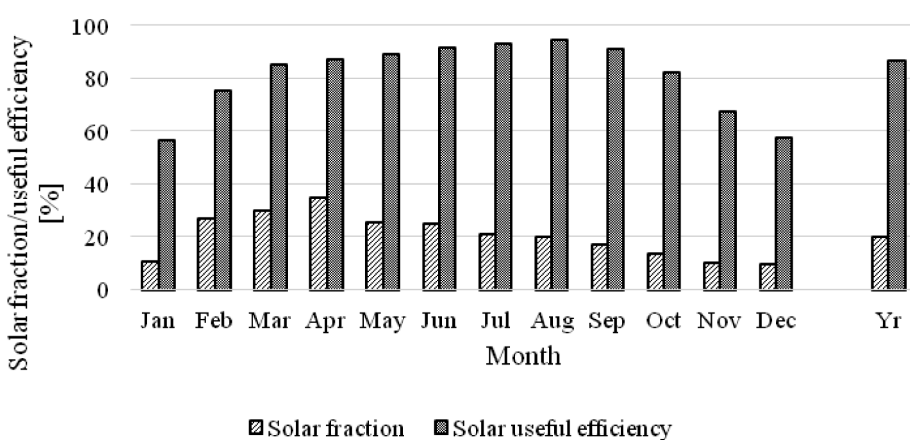

(c) Combined heating and cooling mode

Fig. 12. Monthly and annual solar fraction and solar useful efficiency of Scenario 2.

Either 10 m^2 BISTS on the south façade or 33 m^2 BISTS on the east and west façades are identified to achieve the economic optimum 75% of solar fraction for domestic hot water heating. Even though the DHW load can be fully supplied, the solar efficiencies are low under these circumstances and excessive collector area does not significantly help to increase the solar fraction.

The BISTS on the south façade is primarily recommended for space heating and/or cooling. South-facing collectors provide comparably constant solar gains all year round, resulting in higher load coverage and solar useful efficiency. 64.6% of the heating demand and 20.2% of the cooling requirement can be potentially met by using solar energy. During June and October, the heating demand can be fully covered. But for cooling load, the highest solar fraction is about 35% in April. Since solar availability is in phase with cooling load, the annual solar useful efficiency can be as high as 86% for space cooling but less than 16% for space heating.

Combined heating and cooling enables the system to collect more solar energy and make most use of it. Therefore, it saves more energy from auxiliary heating. Without considering economic factor, Scenario 2, which employs 33 m^2 of east and west collectors (16.5 m^2 on each side) for domestic hot water heating and the remaining BISTS collectors for serving both space heating and cooling, is recommended for the application.

References

[1] S.A. Kalogirou, Solar thermal collectors and applications, Prog. Energy Combust. Sci. 30 (2004) 231–295.
[2] C. Lamnatou, J.D. Mondol, D. Chemisana, C. Maurer, Modelling and simulation of Building-Integrated solar thermal systems: behaviour of the system, Renew. Sustain. Energy Rev. 45 (2015) 36–51.
[3] X.-Y. Sun, X.-D. Sun, X.-G. Li, Z.-Q. Wang, J. He, Performance and building integration of all-ceramic solar collectors, Energy Build. 75 (2014) 176–180.
[4] M.M. Hassan, Y. Beliveau, Design, construction and performance prediction of integrated solar roof collectors using finite element analysis, Constr. Build. Mater. 21 (2007) 1069–1078.
[5] C. Maurer, T. Baumann, M. Hermann, P.D. Lauro, S. Pavan, L. Michel, T.E. Kuhn, Heating and cooling in high-rise buildings using facade-integrated transparent solar thermal collector systems, J. Build. Perform. Simul. 6 (6) (2013) 449–457.
[6] T. Matuska, B. Sourek, Facade solar collectors, Sol. Energy 80 (2006) 1443–1452.
[7] C. Lamnatou, G. Notton, D. Chemisana, C. Cristofari, The environmental performance of a building-integrated solar thermal collector, based on multiple approaches and life-cycle impact assessment methodologies, Build. Environ. 87 (2015) 45–58.
[8] C. Lamnatou, G. Notton, D. Chemisana, C. Cristofari, Life cycle analysis of a building-integrated solar thermal collector, based on embodied energy and embodied carbon methodologies, Energy Build. 84 (2014) 378–387.
[9] F. Motte, G. Notton, C. Cristofari, J.-L. Canaletti, A building integrated solar collector: performance characterization and first stage of numerical calculation, Renew. Energy 49 (2013) 1–5.
[10] A.I. Palmero-Marrero, A.C. Oliveira, Evaluation of a solar thermal system using building louvre shading devices, Sol. Energy 80 (2006) 545–554.
[11] 2011 Buildings Energy Data Book, U.S. Department of Energy, 3 2012 [Online]. Available: http://buildingsdatabook.eren.doe.gov/default.aspx (Accessed 8 March 2015).
[12] C. Lamnatou, J.D. Mondol, D. Chemisana, C. Maurer, Modelling and simulation of Building-Integrated solar thermal systems: behaviour of the coupled building/system configuration, Renew. Sustain. Energy Rev. 48 (2015) 178–191.
[13] “EES: Engineering Equation Solver,” F-Chart Software, LLC., [Online]. Available: http://www.fchart.com/ees/. (Accessed 10 January 2016).
[14] A.I. Palmero-Marrero, A.C. Oliveira, Effect of louver shading devices on building energy requirements, Appl. Energy 87 (2010) 2040–2049.
[15] M. Oishi, T. Noguchi, The evaluation procedure on performance of SDHW system by TRNSYS simulation for a yearly performance prediction, in: Proceedings of Eurosun'2000 on CD-ROM, Copenhagen, Denmark, 2000.
[16] W.A. Beckman, S.A. Klein, J.A. Duffie, Solar Heating Design by the F-chart Method, New York, Wiley/Interscience, 1977.
[17] S.A. Kalogirou, Use of solar parabolic trough collectors for hot water production in Cyprus, a feasibility study, Renew. Energy 2 (2) (1992) 117–124.
[18] W. Sparber, A. Napolitano, P. Melograno, Overview on worldwide installed solar cooling systems, in: Proceedings of 2nd Solar Cooling Conference, Tarragona Costa Dorada, Spain, 2007.
[19] G.A. Florides, S.A. Kalogirou, S.A. Tassou, L.C. Wrobel, Modelling and simulation of an absorption solar cooling system for Cyprus, Sol. Energy 72 (1) (2002) 43–51.
[20] Y. Hang, M. Qu, S. Ukkusuri, Optimizing the design of a solar cooling system using central composite design techniques, Energy Build. 43 (2011) 988–994.
[21] F.J. Kreider, F. Kreith, Solar Energy Handbook, McGrawHill, New York, 1981.
[22] Empire Series Liquid Flat Plate Collector, SunEarth Inc., 2010 [Online]. Available: http://sunearthinc.com/wp-content/uploads/EC-40-1.5-10000551_CERT_2012.pdf (Accessed 14 July 2015).
[23] Solar Rating & Certification Corporation - Solar Facts - Collector Ratings, Solar Rating & Certification Corporation, 2015 [Online]. Available: http://www.solar-rating.org/facts/collector_ratings.html (Accessed 14 July 2015).
[24] TRNSYS 17 Documentation 4.11.1, Solar Energy Laboratory, University of Wisconsin-Madison, Madison, 2009.
[25] Latitude51 Solar Inc, Solar Collector Efficiency [Online]. Available: http://www.latitude51solar.ca/solar-school/solar-school-faq/84-solar-collector-efficiency (Accessed 21 February 2017).
[26] P. Kovacs, Quality Assurance in Solar Heating and Cooling Technology, a Guide to the Standard EN 12975, SP Technical Research Institute of Sweden, 2012.
[27] G. Reysa, Determining Solar Water Heating Collector Flow Rate, Build It Solar, 2015 [Online]. Available: http://www.builditsolar.com/References/ColFlowRate.htm (Accessed 14 July 2015).
[28] “Commercial Reference Buildings,” Office of Energy Efficiency & Renewable Energy, U.S. Department of Energy, [Online]. Available: http://energy.gov/eere/buildings/commercial-reference-buildings. (Accessed 14 July 2015).
[29] R.A. Athalye, Y. Xie, B. Liu, M.I. Rosenberg, Analysis of Daylighting Requirements within ASHRAE Standard 90.1, Pacific Northwest National Laboratory, Richland, Washington 99352, 2013.
[30] L. Li, M. Qu, S. Peng, Performance evaluation of building integrated solar thermal shading system: building energy consumption and daylight provision, Energy Build. 113 (2016) 189–201.
[31] Y. Hang, M. Qu, F. Zhao, Optimization under uncertainty: a case study of a solar absorption cooling and heating system for a medium-sized office building in Atlanta, in: Proceedings of the ASME 2012 6th International Conference on Energy Sustainability, San Diego, 2012.
[32] Estimating the Cost and Energy Efficiency of a Solar Water Heater, U.S. Department of Energy, 2 3 2015 [Online]. Available, http://energy.gov/energysaver/articles/estimating-cost-and-energy-efficiency-solar-water-heater (Accessed 17 September 2015).
[33] A. Walker, Solar water heating, in: 7th Annual North American Passive House Conference, Denver, 2012.
[34] TRNSYS Official Website, Mechanical Engineering Department, The University of Wisconsin, Madison, 2 2013 [Online]. Available: http://sel.me.wisc.edu/trnsys/features/features.html (Accessed 14 July 2015).